ACS APPLIED MATERIALS & INTERFACES

Research Article

www.acsami.org

High-Performance Li–Se Batteries Enabled by Selenium Storage in Bottom-Up Synthesized Nitrogen-Doped Carbon Scaffolds

Hongling Lv,[†,‡] Renpeng Chen,[†,‡] Xiaoqi Wang,[‡] Yi Hu,[‡] Yanrong Wang,[‡] Tao Chen,[‡] Lianbo Ma,[‡] Guoyin Zhu,[‡] Jia Liang,[‡] Zuoxiu Tie,[‡,§] Jie Liu,[‡,⊥] and Zhong Jin*[,‡]

[‡]Key Laboratory of Mesoscopic Chemistry of MOE, School of Chemistry and Chemical Engineering, and [§]College of Engineering and Applied Sciences, Nanjing University, Nanjing, Jiangsu 210023, China

[⊥]Department of Chemistry, Duke University, Durham, North Carolina 27708, United States

Supporting Information

ABSTRACT: Selenium (Se) has great promise to serve as cathode material for rechargeable batteries because of its good conductivity and high theoretical volumetric energy density comparable to sulfur. Herein, we report the preparation of mesoporous nitrogen-doped carbon scaffolds (NCSs) to restrain selenium for advanced lithium–selenium (Li–Se) batteries. The NCSs synthesized by a bottom-up solution-phase method have graphene-like laminar structure and well-distributed mesopores. The unique architecture of NCSs can severe as conductive framework for encapsulating selenium and polyselenides, and provide sufficient pathways to facilitate ion transport. Furthermore, the laminar and porous NCSs can effectively buffer the volume variation during charge/discharge processes. The integrated composite of Se-NCSs has a high Se content and can ensure the complete electrochemical reactions of Se and Li species. When used for Li–Se batteries, the cathodes based on Se-NCSs exhibit high capacity, remarkable cyclability, and excellent rate performance.

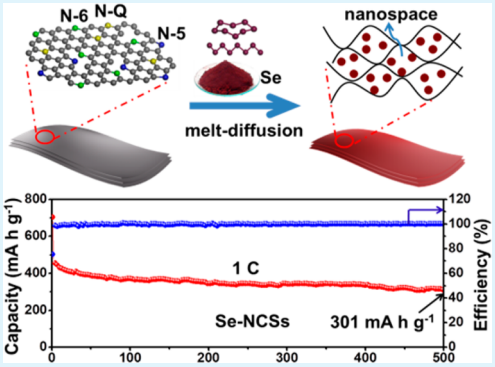

KEYWORDS: *lithium–selenium batteries, selenium cathode, nitrogen-doped carbon scaffolds, electrochemical performances, graphene-like laminar structure*

INTRODUCTION

The increasing demands of portable devices and clean-energy vehicles have largely promoted the broad interest in developing rechargeable batteries.[1−4] However, the existing lithium-ion batteries (LIBs) cannot meet the growing requirements for high energy density and long cycling stability; therefore, next-generation batteries are urgently needed.[5] Sulfur is a potential cathode because of its high theoretical specific capacity (1670 mA h g^{-1}), natural abundance, cheapness, and nontoxicity.[2,5] However, the application of lithium–sulfur (Li–S) batteries is hampered by several drawbacks: (1) because of the low conductivity, sulfur cathodes usually exhibit poor utilization ratio and rate capability; (2) the high solubility of polysulfides in electrolyte leads to low Coulombic efficiency and poor cycling life span.[6−9] To alleviate these problems, great efforts have been made, such as confining sulfur species with conductive polymers,[10−13] nanocarbons,[14−18] or oxide frameworks,[19−21] and looking for suitable electrolytes and additives.[22−24] Although the performances of Li–S batteries have been greatly improved recently, the commercialization is still hindered by the serious capacity fading and poor rate performance.

Selenium is a promising alternative of sulfur. Because of its similar chemical properties to sulfur, selenium can react with lithium to form polyselenides (Li_2Se_x) as well. Compared to sulfur, the theoretical specific capacity of selenium cathode (678 mA g^{-1}) is lower. However, its volumetric capacity density (3278 Ah L^{-1}) is comparable to sulfur (3467 Ah L^{-1}) because of its high density.[25−28] Furthermore, the conductivity of selenium (1×10^{-3} S m^{-1}) is much higher than that of sulfur (5×10^{-28} S m^{-1}), which can lead to higher utilization rate and superior rate performance.[29] These advantages grant selenium the great promise as cathode for constructing secondary batteries with high power density. However, selenium may also suffer from the "shuttle effect" because of the dissolution of Li_2Se_x intermediates in electrolyte.

Several strategies have been proposed to enhance the performance of selenium cathode, such as impregnating selenium into porous carbon matrix[28,30−42] and graphene,[43,44] as listed in Table S1. These reports indicated that carbon frameworks can provide many merits, such as large storage volume, smooth ion transport paths, enhanced conductivity, and buffering the volume variation. Moreover, recent studies have shown that the electrochemical properties of carbon

Received: March 27, 2017
Accepted: July 10, 2017
Published: July 10, 2017

DOI: 10.1021/acsami.7b04321
ACS Appl. Mater. Interfaces 2017, 9, 25232−25238

Scheme 1. Schematics of the Bottom-up Solution-Phase Synthesis of NCSs and the Melt-Diffusion Method To Prepare Se-NCSs

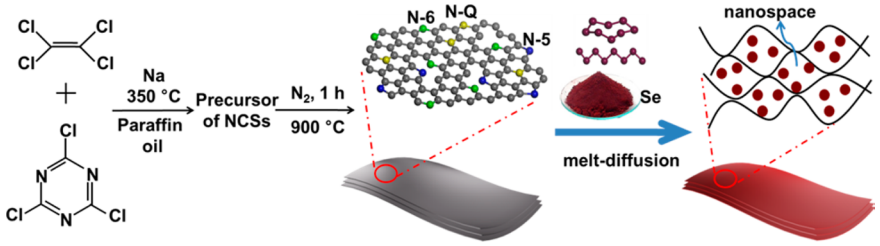

electrode materials can be effectively improved by the doping of heteroatoms.[36,37,45] According to the research of Li−S batteries, the introduction of heteroatoms (e.g., B, S, N, P and O) can improve the interactions between the carbon matrix and intermediate species, thereby suppressing the shuttle effect and boost cycling lifespan.[46−51]

Here we report a novel composite cathode with remarkable electrochemical performance by impregnating selenium into nitrogen-doped carbon scaffolds (NCSs). The obtained Se-NCSs with graphene-like laminar and porous structure can effectively encapsulate selenium, prevent the dissolution of polyselenides (Li_2Se_x), and accommodate the huge volume expansion. As expected, the Se-NCSs exhibits great cycling stability and rate performance far superior to pristine carbon scaffolds (PCSs).

RESULTS AND DISCUSSION

The synthesis procedures of NCSs and Se-NCSs were illustrated in Scheme 1. A bottom-up synthesis approach was modified to prepare the NCSs from nitrogen- and carbon-containing precursors in the solution phase.[52] During the reflux process at 350 °C, the Wurtz coupling reaction accompanied by dechlorination and carbonization was occurred. After the removal of inorganic salts and thermal annealing in N_2 atmosphere, the NCSs with abundant mesopores and laminar structure that composed of stacked wrinkle graphene-like carbon sheets were obtained. After impregnating selenium in NCSs, the nitrogen doping is beneficial for the trapping and charge transfer of Se species; the wrinkled laminar structure can effectively confine selenium and polyselenides and the large pore volume can accommodate the volume change during charge−discharge cycles. Both the NCSs and control sample PCSs stacked by graphene-like carbon sheets with abundant pores show wrinkled laminar structure (Figure 1a, b and Figure S1). Sufficient pathways and large electrode−electrolyte interfaces can be provided by the interconnected carbon framework for electron and ion transport and charge transfer reactions. After selenium loading, the wrinkled laminar morphology of original NCSs became compacted bulk and no selenium accumulation was observed on the surface (Figure 1c), demonstrating the uniform dispersion of Se in the pores of NCSs. The EDX spectrum of Se-NCSs (Figure 1d) indicates the high loading ratio of Se. Combined with the TGA results (Figure S2), the selenium contents are determined to be 56 and 50 wt % for Se-NCSs and Se-PCSs, respectively. The EDX mapping images of carbon and selenium elements are shown in Figure 1e, f, revealing the selenium is uniformly dispersed in Se-NCSs.

To confirm the successful nitrogen doping of NCSs, detailed XPS analysis was performed. The survey XPS spectrum (Figure 2a) shows three distinct peaks representing the energy bands of C 1s, N 1s and O 1s, respectively. The presence of O element

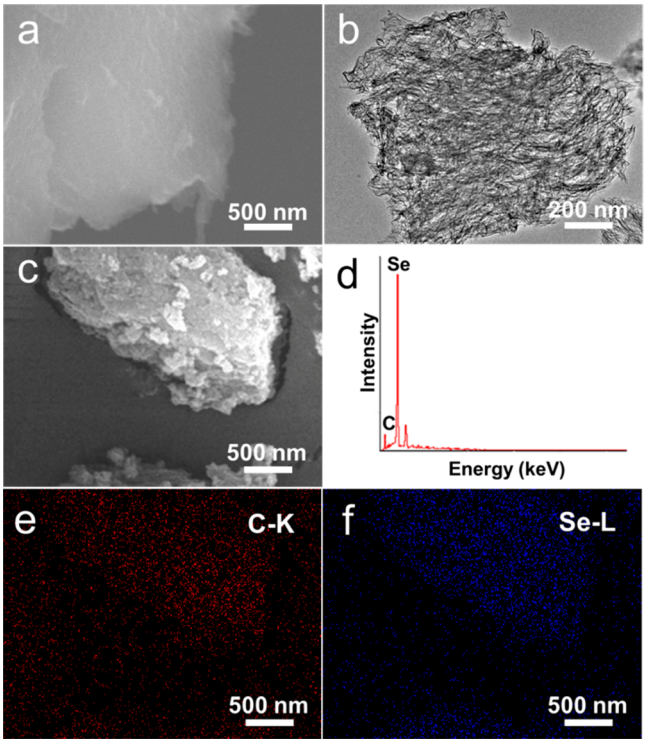

Figure 1. (a) SEM and (b) TEM images of NCSs. (c) SEM image and (d) EDX spectrum of Se-NCSs. (e, f) EDX elemental mapping of carbon and selenium in Se-NCSs.

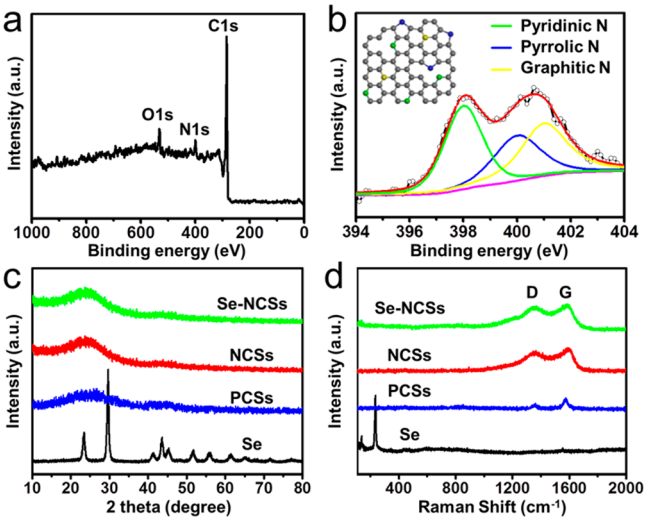

Figure 2. (a) XPS survey spectrum of NCSs. (b) High-resolution XPS spectrum of N 1s region of NCSs, and the inset is the schematic structure of NCSs. (c) XRD patterns and (d) Raman spectra of Se, PCSs, NCSs, and Se-NCSs, respectively.

DOI: 10.1021/acsami.7b04321
ACS Appl. Mater. Interfaces 2017, 9, 25232−25238

was ascribed to the physicochemical adsorption of trace-amount oxygen during synthesis. The atomic content of N in NCSs was estimated to be 6.5 wt %. As shown in Figure 2b, the high-resolution N 1s spectrum of NCSs can be divided into three individual peaks: pyridinic N (398.2 eV), pyrrolic N (400.1 eV) and graphitic N (401.0 eV), indicating the presence of nitrogen-containing pentatomic rings, hexatomic rings, and defects in NCSs. According to the XPS analysis, a possible structure illustration of NCSs was given by the inset of Figure 2b. The electrochemical activity can be enhanced by the nitrogen heteroatoms in carbon matrix,[53,54] which is conducive to the electrochemical performance of Se-NCSs.

Figure 2c shows the XRD patterns of Se, PCSs, NCSs and Se-NCSs. Both the NCSs and Se-NCSs show two broad peaks of (002) and (101), suggesting the amorphous state of carbon. No obvious selenium peaks were observed in the XRD curve of Se-NCSs, demonstrating that selenium was confined as highly dispersed and tiny nanoparticles in NCSs.[45,55] To further investigate the interactions between Se and NCSs, we characterized the samples by Raman spectroscopy (Figure 2d). For pure Se, three Raman characteristic peaks at 138, 236, and 458 cm^{-1} were observed, demonstrating the presence of chain-structured and annular selenium.[56] For NCSs, the G band (associated with graphitic carbon) and D band (related to defects or disorders) are located at 1591 and 1356 cm^{-1}, whereas PCSs show a G band and a D band at 1574 and 1356 cm^{-1}, respectively. The intensity ratios of D/G bands of NCSs and PCSs calculated from the Raman spectra were 0.84 and 0.73, respectively, indicating the both samples were partially graphitized, thus favoring to the conductivity and electron transport. Previous works reported that an appropriate degree of nitrogen doping could result in a better conductivity.[57,58] Moreover, the powder electronic conductivity of NCSs and PCSs measured with a multifunctional powder resistivity tester (FT-301, with a mold of 4 mm diameter) are 660.7 and 525.0 S m^{-1}, respectively, further demonstrating the higher conductivity of NCSs. After selenium loading, no apparent Raman peaks of selenium could be observed, indicating that selenium was uniformly encapsulated and dispersed in the NCSs,[45,55] in agreement with the EDX and XRD results.

The pore structures of NCSs, Se-NCSs, PCSs, and Se-PCSs were investigate by the nitrogen adsorption−desorption isotherms (Figure 3). The BET surface area and pore volume of NCSs are 615 $m^2\ g^{-1}$ and 1.36 $cm^3\ g^{-1}$, respectively. Based on the pore volume, the maximum selenium loading content can reach 86.7%. For accommodating the volume expansion caused by charging and ensure the infiltration of electrolyte, sufficient space was provided by setting the typical selenium content in Se-NCSs to 56 wt % (Figure S2). After the encapsulating selenium, the BET surface area and pore volume of the Se-NCSs composite decrease to 56 $m^2\ g^{-1}$ and 0.36 $cm^3\ g^{-1}$. Moreover, the pore distribution curve of Se-NCSs showed no sharp peak, indicating a large portion of the mesopores had been filled with selenium. As shown in Figure 3c, d, the PCSs and Se-PCSs showed similar pore structure parameters compared to NCSs and Se-NCSs, respectively. The wrinkled laminar structures with abundant mesopores can serve as conductive framework for encapsulating selenium and polyselenides, and also provide sufficient pathways to facilitate ionic migration. As presented in Figure S3, the binding energies of Se $3d_{3/2}$ and $3d_{5/2}$ in the XPS spectrum of Se-NCSs are higher than those of Se-PCSs, indicating a relatively stronger affinity between the NCSs and Se.

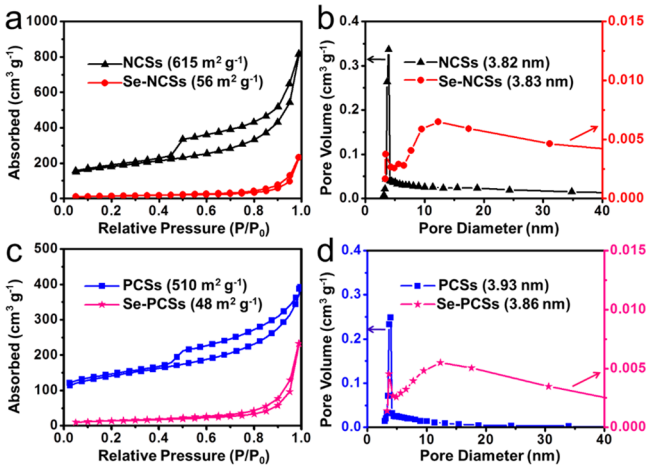

Figure 3. (a) Nitrogen adsorption−desorption isotherms and (b) pore size distributions of NCSs and Se-NCSs, respectively. (c) Nitrogen adsorption−desorption isotherms and (d) pore size distributions of PCSs and Se-PCSs, respectively.

Coin cells (standard type-2032) were assembled to compare the electrochemical performances of the as-obtained electrodes. Figure 4a displays the typical CV curves of Se-NCSs based

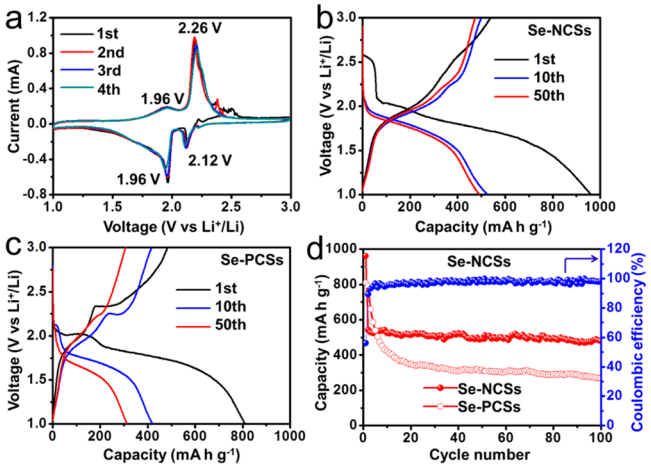

Figure 4. (a) CV curves of Se-NCSs at a sweep rate of 0.2 mV s^{-1}. (b, c) Charge/discharge profiles of Se-NCSs and Se-PCSs based electrodes at 0.1 *C*. (d) Cycling performance of Se-NCSs and Se-PCSs and corresponding Coulombic efficiency of Se-NCSs based cathode at 0.1 *C*.

electrode in the voltage range of 1.0−3.0 V with a sweep rate of 0.2 mV s^{-1}. In the first cycle, two obvious cathodic peaks appeared at 2.12 and 1.96 V, corresponding to the reduction from Se to polyselenides and then to Li_2Se, respectively. The subsequent anodic scan exhibited two anodic peaks at 1.96 and 2.26 V, corresponding to the reversible conversions from Li_2Se to polyselenides and then to Se, respectively.[59] In the following scans, the CV curves are almost overlapped, indicating the high reversibility and stability. This indicated that the NCSs was quite effective for confining both Se and polyselenides during redox cycles.

To investigate the cycling stability of Se-NCSs and Se-PCSs based cathodes, we performed galvanostatic charge/discharge tests at 0.1 *C* (1 *C* = 678 mA g^{-1} based on theoretical specific capacity of Se), as shown in Figure 4b, c. In the first cycle, the

DOI: 10.1021/acsami.7b04321
ACS Appl. Mater. Interfaces 2017, 9, 25232−25238

Se-NCSs based cathode exhibited a high capacity of 960 mA h g^{-1} and a reversible capacity of 538 mA h g^{-1}. In the following 10th and 50th cycles, the specific capacity became stable. The discharge curves of Se-NCSs delivered only one sloping voltage plateau, similar to some previous works.[37,60] This result is mainly due to the volume confinement effect of the NCSs with abundant pores and wrinkled laminar structure, in which the uniformly dispersed selenium was prevented to form higher order polyselenides.[60] As control samples, the charge/discharge profiles of NCSs and PCSs without the loading of selenium showed very low capacities (Figure S4), indicating that the high capacity of Se-NCSs and Se-PCSs are mainly contributed from the encasulated selenium.

The Se-PCSs based electrode exhibited similar electrochemical behavior compared to Se-NCSs and delivered a high initial reversible capacity (Figure 4c). However, the capacity of Se-PCSs based electrode decreased rapidly in the initial 50 cycles. The cycling performances of Se-NCSs and Se-PCSs based cathodes are shown in Figure 4d. The Se-NCSs based cathode kept a reversible capacity of 480 mA h g^{-1} after 100 cycles and a corresponding Coulombic efficiency over 96%. In contrast, the Se-PCSs based cathode exhibited a much lower capacity of 268 mA h g^{-1} after 100 cycles.

Electrochemical impedance spectroscopy (EIS) measurements were carried out for Se-NCSs and Se-PCSs based electrodes before and after 100 cycles at 0.1 C. Figure S5 shows that the fresh electrode of Se-NCSs exhibited a charge transfer resistance lower than that of Se-PCSs, indicting the electrical conductivity was improved by the introduction of N heteroatoms. After 100 cycles, the charge transfer resistance of Se-NCSs electrode further decreased. The improved conductivity of electrodes after the charge/discharge processes should be attributed to the wetting and infiltration of electrolyte into electrode.[55,61−63] Compared to Se-PCSs, the superior conductivity of Se-NCSs can facilitate electron transport and lead to lower polarization, thus beneficial to electrochemical performance and stability.[45]

The rate performances of Se-NCSs and Se-PCSs based cathodes were presented in Figure 5a, b and Figure S6a. For Se-NCSs based cathode, the reversible capacity reached 475 mA h g^{-1} at the rate of 0.2 *C*. As the current density raised to 2 *C*, the reversible capacity kept at 275 mA h g^{-1} (~58% retention of the capacity at 0.2 *C*). After the rate was set back to 0.2 *C*, the reversible capacity went back to 450 mA h g^{-1}, demonstrating excellent reversibility and stability. In contrast, the Se-PCSs based cathode only delivered a low capacity of 170 mA h g^{-1} at 2 *C*. When the current density was set back to 0.2 *C*, the specific capacity of Se-PCSs cathode recovered to 251 mA h g^{-1} after cycling at different rates. Notably, the cathode based on Se-NCSs exhibited incredible cycle stability and excellent reversibility. To assess the long-term cyclability, the cathodes were tested for 500 cycles at 1 *C* (Figure 5c and Figure S6b). For Se-NCSs cathode, the discharge capacity was 457 mA h g^{-1} at the second cycle and retained 301 mA h g^{-1} after 500 cycles, corresponding to a capacity retention of 66% and a low average capacity decay of 0.068% per cycle. The Coulombic efficiency kept at nearly 100% throughout the cycling, indicative of a prolonged cycle life. In comparison, Se-PCSs electrode only delivered a capacity of 98 mA h g^{-1} at 1 C after 500 cycles. We also compared the performance of Se-NCSs with other reported Se−C composite cathodes for Li−Se batteries, as presented in Table S1. The Se-NCSs electrode exhibits good performances superior or comparable to other Se-based electrodes in the previous works (Table S1),[28,30−44] demonstrating the remarkable lithium storage properties of Se-NCSs.

Moreover, control samples with different nitrogen content were obtained by annealing the carbon scaffolds precursor at 800 and 1000 °C, and named as NCSs-800 and NCSs-1000, respectively. The nitrogen content of NCSs-800 and NCSs-1000 are measured to be 7.2 and 4.8 wt %, respectively, according to the XPS results (Figure S7). After loading with the same ratio of selenium, the cycling performance of Se-NCSs-800 and Se-NCSs-1000 cathodes are presented in Figure S8. The performance of Se-NCSs-800 and Se-NCSs-1000 cathodes are inferior to that of Se-NCSs annealed at 900 °C, indicating that the electrode performance can be affected by the annealing temperature and nitrogen content.

The enhanced capacity retention and rate performance of Se-NCSs should be ascribed to the introduction of N heteroatoms, which increased the conductivity and decreased the polarization. Moreover, the introduction of N atoms can accelerate lithium insertion and enhance the interaction between the NCSs and lithium polyselenides.[59,64] These results further illustrated the superiorities of NCSs for accommodating volume change, maintaining good structural stability, and restraining the diffusion of polyselenides during long-term cycling.

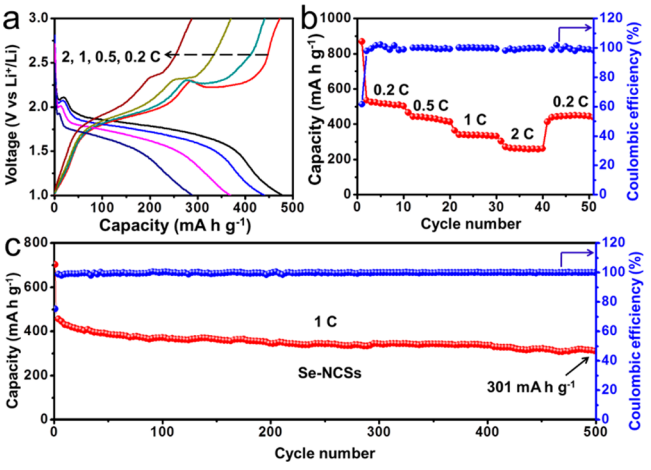

Figure 5. (a) Charge/discharge profiles and (b) rate capability of Se-NCSs based cathode at 0.2−2 *C*. (c) Long-term cycling performance and corresponding Coulombic efficiency of Se-NCSs based cathode at 1 *C*.

CONCLUSION

In this work, a novel strategy is demonstrated to prepare the composite of Se-NCSs for rechargeable Li−Se batteries. The unique framework of NCSs with favorable pore structure and improved conductivity can effectively confine selenium and polyselenides, thus lead to high capacity and long-term cyclability. On the basis of the outstanding electrochemical performances, the NCSs should be considered as a promising selenium host material to develop high-performance lithium−selenium batteries.

EXPERIMENTAL SECTION

Material Synthesis. Synthesis of NCSs: A bottom-up solution-phase method modified from previous work[52] was developed to prepare the NCSs. Typically, 100 mL of paraffin oil was poured into a dry three-neck round-bottom flask (200 mL) stocked with an air reflux condenser. Then, 2.5 mL of tetrachloroethylene, 3.7 g of cyanuric

DOI: 10.1021/acsami.7b04321
ACS Appl. Mater. Interfaces 2017, 9, 25232−25238

chloride, and 5.0 g of chopped sodium metal were put into the flask under N_2 protection. The flask was heated to 350 °C under continuous stirring and refluxed for 6 h with N_2 protection. After cooling down to ambient temperature, the mixture was filtered through PTFE membrane and sequentially washed with petroleum ether, acetone, deionized water and ethanol to get rid of residual salts and organic compounds. After dried under vacuum at 120 °C, the brown solid product was annealed in an electric furnace under Ar atmosphere for 1 h at 900 °C with a ramp rate of 2 °C min^{-1}. The resulting NCSs solid was ground to powder. Control samples with different nitrogen content were also obtained by annealing the product at 800 and 1000 °C, and named as NCSs-800 and NCSs-1000, respectively.

Synthesis of PCSs: For comparison, PCSs without nitrogen heteroatoms were prepared as a control sample through the same synthesis process as above, except for less sodium (2.5 g) and no cyanuric chloride (nitrogen source) were used.

Impregnation of selenium in carbon frameworks: The composites of Se-NCSs or Se-PCSs were prepared by a melt-diffusion method. First, 0.4 g NCSs or PCSs were ground with 0.6 g Se for 1 h. The mixture was then kept at 280 °C for 12 h in a stainless-steel autoclave to facilitate the diffusion and encapsulation of melted selenium in the pores of NCSs or PCSs. Finally, the resultant Se-NCSs and Se-PCSs were collected as black powder.

Instruments and Characterizations. The morphologies of products were characterized with a scanning electron microscope (SEM, Hitachi S-4800) equipped with an energy-dispersive X-ray spectroscope (EDX). Transmission electron microscopy (TEM) observation was performed on a JEM-2100 instrument. Powder X-ray diffraction spectra (XRD) were measured by an X-ray diffractometer (Bruker D-8 Advance, Cu Kα radiation at 40 kV and 40 mA). Thermogravimetric analysis (TGA, Netzsch STA 449 C) was carried out in a N_2 atmosphere with a heating rate of 10 °C per minute. X-ray photoelectron spectra (XPS) were collected using a PHI-5000 VersaProbe X-ray photoelectron spectrometer with an Al Kα X-ray radiation. Raman spectra were collected with a Horiba JY Evolution Raman spectrometer (532 nm laser source). Nitrogen adsorption−desorption isotherms were measured through Brunauer−Emmett−Teller (BET) analysis on a Quantachrome Autosorb-IQ-2Canalyzer at liquid N2 temperature.

Electrochemical Measurements. The cathodes based on Se-NCSs or Se-PCSs were prepared as follows. Se-NCSs or Se-PCSs (80 wt %), super P (10 wt %), and sodium alginate (10 wt %) were mixed and stirred in distilled water to form a slurry, then casted on Al foil and dried in vacuum at 100 °C for 12 h. The loading weight of active material is 0.8−1.0 mg cm^{-2}. The Li−Se batteries were assembled with Celgard-2400 separators and Li foil anodes in an Ar-filled glovebox. The electrolyte is 1.0 M of bis(trifluoromethane) sulfonimide lithium (LiTFSI) in a mixed solvent of dimethoxyethane and dioxolane (1:1 by volume). Galvanostatic charge/discharge tests were performed between 1.0−3.0 V vs Li^+/Li on a Wuhan Land-CT2001 system. Cyclic voltammetry (CV) was performed using an electrochemistry workstation (Chenhua CHI-760E) at a scan rate of 0.2 mV s^{-1}. The specific capacity was based on the loading mass of selenium.

■ ASSOCIATED CONTENT

Supporting Information

The Supporting Information is available free of charge on the ACS Publications website at DOI: 10.1021/acsami.7b04321.

Comparison of lithium storage performances of Se-NCSs cathode with other Se−C composite cathodes in the literature; SEM and TEM images of PCSs; thermal analysis curves of Se-NCSs and Se-PCSs; XPS spectra at Se 3d region of Se-NCSs and Se-PCSs; charge/discharge profiles of NCSs and PCSs at a current density of 60 mA g^{-1}; Nyquist plots of the Li−Se cells with different Se composite cathodes after 100 cycles at 0.1 *C*; rate capability of Se-PCSs based cathode at 0.2−2*C*; long-term cycling performance of Se-PCSs based cathode at 1 *C*; XPS spectra of NCSs-800 and PCSs-1000; cycling performance of Se-NCSs-800- and Se-NCSs-100-based cathodes at 0.1 *C* (PDF)

■ AUTHOR INFORMATION

Corresponding Author

*E-mail: zhongjin@nju.edu.cn. Phone: +86-18115605182.

ORCID

Tao Chen: 0000-0003-2536-4145

Jie Liu: 0000-0003-0451-6111

Zhong Jin: 0000-0001-8860-8579

Author Contributions

†H.L. and R.C. contributed equally to this work.

Notes

The authors declare no competing financial interest.

■ ACKNOWLEDGMENTS

This work was supported by National Key Research and Development Program of China (2017YFA0208200, 2016YFB0700600), National Key Basic Research Program (2015CB659300), Projects of NSFC (21403105, 21573108), Fundamental Research Funds for the Central Universities (020514380107), and a project funded by the Priority Academic Program Development of Jiangsu Higher Education Institutions.

■ REFERENCES

(1) Goodenough, J. B.; Park, K. S. The Li-ion Rechargeable Battery: a Perspective. *J. Am. Chem. Soc.* **2013**, *135*, 1167−1176.

(2) Manthiram, A.; Fu, Y. Z.; Su, Y. S. Challenges and Prospects of Lithium−sulfur Batteries. *Acc. Chem. Res.* **2013**, *46*, 1125−1134.

(3) Bruce, P. G.; Scrosati, B.; Tarascon, J. M. Nanomaterials for Rechargeable Lithium Batteries. *Angew. Chem., Int. Ed.* **2008**, *47*, 2930−2946.

(4) Wang, Y. R.; Chen, R. P.; Chen, T.; Lv, H. L.; Zhu, G. Y.; Ma, L. B.; Wang, C. X.; Jin, Z.; Liu, J. Emerging Non-lithium Ion Batteries. *Energy Storage Mater.* **2016**, *4*, 103−129.

(5) Bruce, P. G.; Freunberger, S. A.; Hardwick, L. J.; Tarascon, J. M. Li−O_2 and Li−S Batteries with High Energy Storage. *Nat. Mater.* **2012**, *11*, 19−29.

(6) Ji, X.; Lee, K. T.; Nazar, L. F. A Highly Ordered Nanostructured Carbon-sulphur Cathode for Lithium-sulphur Batteries. *Nat. Mater.* **2009**, *8*, 500−506.

(7) Li, G. C.; Li, G. R.; Ye, S. H.; Gao, X. P. A Polyaniline-Coated Sulfur/Carbon Composite with an Enhanced High-Rate Capability as a Cathode Material for Lithium/Sulfur Batteries. *Adv. Energy Mater.* **2012**, *2*, 1238−1245.

(8) Chung, S. Y.; Bloking, J. T.; Chiang, Y. M. Electronically Conductive Phospho-olivines as Lithium Storage Eectrodes. *Nat. Mater.* **2002**, *1*, 123−128.

(9) Cheon, S. E.; Ko, K. S.; Cho, J. H.; Kim, S. W.; Chin, E. Y.; Kim, H. T. Rechargeable lithium sulfur battery I. Structural Change of Sulfur Cathode during Discharge and Charge. *J. Electrochem. Soc.* **2003**, *150*, A796−A799.

(10) Xiao, L. F.; Cao, Y. L.; Xiao, J.; Schwenzer, B.; Engelhard, M. H.; Saraf, L. V.; Nie, Z. M.; Exarhos, G. J.; Liu, A. Soft Approach to Encapsulate Sulfur: Polyaniline Nanotubes for Lithium-sulfur Batteries with Long Cycle Life. J. *Adv. Mater.* **2012**, *24*, 1176−1181.

(11) Zhou, W.; Yu, Y.; Chen, H.; DiSalvo, F. J.; Abruña, H. D. Yolk−shell Structure of Polyaniline-coated Sulfur for Lithium−sulfur Batteries. *J. Am. Chem. Soc.* **2013**, *135*, 16736−16743.

(12) Liang, X.; Liu, Y.; Wen, Z. Y.; Huang, L. Z.; Wang, X. Y.; Zhang, H. A Nano-structured and Highly Ordered Polypyrrole-sulfur Cathode for Lithium−sulfur Batteries. *J. Power Sources* **2011**, *196*, 6951−6955.

DOI: 10.1021/acsami.7b04321
ACS Appl. Mater. Interfaces 2017, 9, 25232−25238

(13) Ma, G. Q.; Wen, Z. Y.; Jin, J.; Lu, Y.; Wu, X. W.; Wu, M. F.; Chen, C. H. Hollow Polyaniline Sphere@ sulfur Composites for Prolonged Cycling Stability of Lithium−sulfur Batteries. *J. Mater. Chem. A* **2014**, *2*, 10350−10354.
(14) Schuster, J.; He, G.; Mandlmeier, B.; Yim, T.; Lee, K. T.; Bein, T.; Nazar, L. F. Spherical Ordered Mesoporous Carbon Nanoparticles with High Porosity for Lithium−sulfur Batteries. *Angew. Chem., Int. Ed.* **2012**, *51*, 3591−3595.
(15) Zhang, B.; Qin, X.; Li, G. R.; Gao, X. P. Enhancement of Long Stability of Sulfur Cathode by Encapsulating Sulfur into Micropores of Carbon Spheres. *Energy Environ. Sci.* **2010**, *3*, 1531−1537.
(16) Elazari, R.; Salitra, G.; Garsuch, A.; Panchenko, A.; Aurbach, D. Sulfur-impregnated Activated Carbon Fiber Cloth as a Binder-free Cathode for Rechargeable Li-S batteries. *Adv. Mater.* **2011**, *23*, 5641−5644.
(17) Li, N. W.; Zheng, M. B.; Lu, H. L.; Hu, Z. B.; Shen, C. F.; Chang, X. F.; Ji, G. B.; Cao, J. M.; Shi, Y. High-rate Lithium−sulfur Batteries Promoted by Reduced Graphene Oxide Coating. *Chem. Commun.* **2012**, *48*, 4106−4108.
(18) Zheng, G. Y.; Zhang, Q. F.; Cha, J. J.; Yang, Y.; Li, W. Y.; Seh, Z. W.; Cui, Y. Amphiphilic Surface Modification of Hollow Carbon Nanofibers for Improved Cycle Life of Lithium Sulfur Batteries. *Nano Lett.* **2013**, *13*, 1265−1270.
(19) Liang, Z.; Zheng, G. Y.; Li, W. Y.; Seh, Z. W.; Yao, H. B.; Yan, K.; Kong, D. S.; Cui, Y. Sulfur Cathodes with Hydrogen Reduced Titanium Dioxide Inverse Opal Structure. *ACS Nano* **2014**, *8*, 5249−5256.
(20) Wei Seh, Z. W.; Li, W. Y.; Cha, J. J.; Zheng, G. Y.; Yang, Y.; McDowell, M. T.; Hsu, P.; Cui, Y. Sulphur−TiO_2 Yolk−shell Nanoarchitecture with Iinternal Void Space for Long-cycle Lithium−sulphur Batteries. *Nat. Commun.* **2013**, *4*, 1331−1336.
(21) Liang, X.; Hart, C.; Pang, Q.; Garsuch, A.; Weiss, T.; Nazar, L. F. A Highly Efficient Polysulfide Mediator for Lithium−sulfur Batteries. *Nat. Commun.* **2015**, *6*, 5682−5689.
(22) Suo, L.; Hu, Y. S.; Li, H.; Armand, M.; Chen, L. A New Class of Solvent-in-salt Electrolyte for High-energy Rechargeable Metallic Lithium Batteries. *Nat. Commun.* **2013**, *4*, 1481−1489.
(23) Ji, L.; Rao, M.; Zheng, H.; Zhang, L.; Li, Y.; Duan, W.; Guo, J.; Cairns, E. J.; Zhang, Y. Graphene Oxide as a Sulfur Immobilizer in High Performance Lithium/Sulfur Cells. *J. Am. Chem. Soc.* **2011**, *133*, 18522−18525.
(24) Liang, X.; Wen, Z.; Liu, Y.; Wu, M.; Jin, J.; Zhang, H.; Wu, X. Improved Cycling Performances of Lithium Sulfur Batteries with $LiNO_3$-Modified Electrolyte. *J. Power Sources* **2011**, *196*, 9839−9843.
(25) Yang, C. P.; Yin, Y. X.; Guo, Y. G. Elemental Selenium for Electrochemical Energy Storage. *J. Phys. Chem. Lett.* **2015**, *6*, 256−266.
(26) Zhang, S. F.; Wang, W. P.; Xin, S.; Ye, H.; Yin, Y. X.; Guo, Y. G. Graphitic Nanocarbon−Selenium Cathode with Favorable Rate Capability for Li−Se Batteries. *ACS Appl. Mater. Interfaces* **2017**, *9*, 8759−8765.
(27) Abouimrane, A.; Dambournet, D.; Chapman, K. W.; Chupas, P. J.; Weng, W.; Amine, K. A New Cass of Lithium and Sodium Rechargeable Batteries Based on Selenium and Selenium−sulfur as a Positive Electrode. *J. Am. Chem. Soc.* **2012**, *134*, 4505−4508.
(28) Luo, C.; Xu, Y. H.; Zhu, Y. J.; Liu, Y. H.; Zheng, S. Y.; Liu, Y.; Langrock, A.; Wang, C. S. Selenium@ mesoporous Carbon Composite with Superior Lithium and Sodium Storage Capacity. *ACS Nano* **2013**, *7*, 8003−8010.
(29) Yang, C. P.; Xin, S.; Yin, Y. X.; Ye, H.; Zhang, J.; Guo, Y. G. An Advanced Selenium−carbon Cathode for Rechargeable Lithium−selenium Batteries. *Angew. Chem., Int. Ed.* **2013**, *52*, 8363−8367.
(30) Jiang, S. F.; Zhang, Z. A.; Lai, Y. Q.; Qu, Y. H.; Wang, X. W.; Li, J. Selenium Encapsulated into 3D Interconnected Hierarchical Porous Carbon Aerogels for Lithium−selenium Batteries with High rate Performance and Cycling Stability. *J. Power Sources* **2014**, *267*, 394−404.
(31) Liu, L.; Wei, Y. J.; Zhang, C. F.; Zhang, C.; Li, X.; Wang, J. T.; Ling, L. C. Enhanced Electrochemical Performances of Mesoporous Carbon Microsphere/Selenium Composites by Controlling the Pore Structure and Nitrogen Doping. *Electrochim. Acta* **2015**, *153*, 140−148.
(32) Lai, Y. Q.; Gan, Y. Q.; Zhang, Z. A.; Chen, W.; Li. Metal-organic Frameworks-derived Mesoporous Carbon for High Performance Lithium−selenium Battery. *Electrochim. Acta* **2014**, *146*, 134−141.
(33) Zhang, J.; Zhang, Z. A.; Li, Q.; Qu, Y. H.; Jiang, S. F. Selenium Encapsulated into Interconnected Polymer-derived Porous Carbon Nanofiber Webs as Cathode Materials for Lithium-selenium Batteries. *J. Electrochem. Soc.* **2014**, *161*, A2093−A2098.
(34) Liu, Y. X.; Si, L.; Zhou, X. S.; Liu, X.; Xu, Y.; Bao, J. C.; Dai, Z. H. A Selenium-confined Microporous Carbon Cathode for Ultrastable Lithium−selenium Batteries. *J. Mater. Chem. A* **2014**, *2*, 17735−17739.
(35) Ye, H.; Yin, Y. X.; Zhang, S. F.; Guo, Y. G. Advanced Se−C Nanocomposites: a Bifunctional Electrode Material for Both Li−Se and Li-ion Batteries. *J. Mater. Chem. A* **2014**, *2*, 13293−13298.
(36) Qu, Y. H.; Zhang, Z. A.; Jiang, S. F.; Wang, X. W.; Lai, Y. Q.; Liu, Y. X.; Li, J. Confining Selenium in Nitrogen-containing Hierarchical Porous Carbon for High-rate Rechargeable Lithium−selenium Batteries. *J. Mater. Chem. A* **2014**, *2*, 12255−12261.
(37) Yi, Z. Q.; Yuan, L. X.; Sun, D.; Li, Z.; Wu, C.; Yang, W. J.; Wen, Y. W.; Shan, B.; Huang, Y. H. High-performance Lithium−selenium Batteries Promoted by Heteroatom-doped Microporous Carbon. *J. Mater. Chem. A* **2015**, *3*, 3059−3065.
(38) Zhang, J. J.; Fan, L.; Zhu, Y. C.; Xu, Y. H.; Liang, J. W.; Wei, D. H.; Qian, Y. T. Selenium/Interconnected Porous Hollow Carbon Bubbles Composites as the Cathodes of Li−Se Batteries with High Performance. *Nanoscale* **2014**, *6*, 12952−12957.
(39) Wang, H. Q.; Li, S.; Chen, Z. X.; Liu, H. K.; Guo, Z. P. A Novel Type of One-dimensional Organic Selenium-containing Fiber with Superior Performance for Lithium−selenium and Sodium−selenium Batteries. *RSC Adv.* **2014**, *4*, 61673−61678.
(40) Zeng, L. C.; Zeng, W. C.; Jiang, Y.; Wei, X.; Li, W. H.; Yang, C. L.; Zhu, Y. W.; Yu, Y. A Flexible Porous Carbon Nanofibers-Selenium Cathode with Superior Electrochemical Performance for Both Li-Se and Na-Se Batteries. *Adv. Energy Mater.* **2015**, *5*, 1401377.
(41) Luo, C.; Wang, J. J.; Suo, L. M.; Mao, J. F.; Fan, X. L.; Wang, C. S. In Situ Formed Carbon Bonded and Encapsulated Selenium Composites for Li−Se and Na−Se Batteries. *J. Mater. Chem. A* **2015**, *3*, 555−561.
(42) Zhang, Z. A.; Yang, X.; Guo, Z. P.; Qu, Y. H.; Li, J.; Lai, Y. Q. Selenium/Carbon-rich Core−shell Composites as Cathode Materials for Rechargeable Lithium−selenium Batteries. *J. Power Sources* **2015**, *279*, 88−93.
(43) Han, K.; Liu, Z.; Ye, H. Q.; Dai, F. Flexible Self-standing Graphene−Se@ CNT composite Film as a Binder-free Cathode For Rechargeable Li−Se Batteries. *J. Power Sources* **2014**, *263*, 85−89.
(44) He, J. R.; Chen, Y. F.; Lv, W. Q.; Wen, K. C.; Li, P. J.; Wang, Z. G.; Zhang, W. L.; Qin, W.; He, W. D. Three-dimensional Hierarchical Graphene-CNT@ Se: a Highly Efficient Freestanding Cathode for Li−Se Batteries. *ACS Energy Lett.* **2016**, *1*, 16−20.
(45) Jiang, Y.; Ma, X. J.; Feng, J. K.; Xiong, S. L. Selenium in Nitrogen-doped Microporous Carbon Spheres for High-performance Lithium−selenium Batteries. *J. Mater. Chem. A* **2015**, *3*, 4539−4546.
(46) Sun, F. G.; Wang, J. T.; Chen, H. C.; Li, W. C.; Qiao, W. M.; Long, D. H.; Ling, L. C. High Efficiency Immobilization of Sulfur on Nitrogen-enriched Mesoporous Carbons for Li−S Batteries. *ACS Appl. Mater. Interfaces* **2013**, *5*, 5630−5638.
(47) Chen, J. J.; Yuan, R. M.; Feng, J. M.; Zhang, Q.; Huang, J. X.; Fu, G.; Zheng, M. S.; Ren, B.; Dong, Q. F. Conductive Lewis Base Matrix to Recover the Missing Link of Li_2S_8 during the Sulfur Redox Cycle in Li−S Battery. *Chem. Mater.* **2015**, *27*, 2048−2055.
(48) Cao, Y.; Li, X. L.; Zheng, M. S.; Yang, M. P.; Yang, X. L.; Dong, Q. F. Ultra-high Rates and Reversible Capacity of Li-S Battery with a Nitrogen-doping Conductive Lewis Base Matrix. *Electrochim. Acta* **2016**, *192*, 467−474.
(49) Hulicova-Jurcakova, D.; Seredych, M.; Lu, G. Q.; Bandosz, T. J. Combined Effect of nitrogen- and oxygen-containing Functional Groups of Microporous Activated Carbon on Its Electrochemical

DOI: 10.1021/acsami.7b04321
ACS Appl. Mater. Interfaces 2017, 9, 25232−25238

Performance in Supercapacitors. *Adv. Funct. Mater.* **2009**, *19*, 438−447.
(50) Chen, L. F.; Zhang, X. D.; Liang, H. W.; Kong, M.; Guan, Q. F.; Chen, P.; Wu, Z. Y.; Yu, S. H. Synthesis of Nitrogen-doped Porous Carbon Nanofibers as an Efficient Electrode Material for Supercapacitors. *ACS Nano* **2012**, *6*, 7092−7102.
(51) Song, J.; Xu, T.; Gordin, M. L.; Zhu, P.; Lv, D.; Jiang, Y.; Chen, Y.; Duan, Y.; Wang, D. H. Nitrogen-Doped Mesoporous Carbon Promoted Chemical Adsorption of Sulfur and Fabrication of High-Areal-Capacity Sulfur Cathode with Exceptional Cycling Stability for Lithium-Sulfur Batteries. *Adv. Funct. Mater.* **2014**, *24*, 1243−1250.
(52) Jin, Z.; Sun, Z. Z.; Simpson, L. J.; O'Neill, K. J.; Parilla, P. A.; Li, Y.; Stadie, N. P.; Ahn, C. C.; Kittrell, C.; Tour, J. M. Solution-phase Synthesis of Heteroatom-substituted Carbon Scaffolds for Hydrogen storage. *J. Am. Chem. Soc.* **2010**, *132*, 15246−15251.
(53) Wu, Z. S.; Ren, W. C.; Xu, L.; Li, F.; Cheng, H. M. Doped Graphene Sheets as Anode Materials with Superhigh Rate and Large Capacity for Lithium ion Batteries. *ACS Nano* **2011**, *5*, 5463−5471.
(54) Qie, L.; Chen, W. M.; Wang, Z. H.; Shao, Q. G.; Li, X.; Yuan, L. X.; Hu, X. L.; Zhang, W. X.; Huang, Y. H. Nitrogen-doped Porous Carbon Nanofiber Webs as Anodes for Lithium Ion Batteries with a Superhigh Capacity and Rate Capability. *Adv. Mater.* **2012**, *24*, 2047−2050.
(55) Han, K.; Liu, Z.; Shen, J. M.; Lin, Y. Y.; Dai, F.; Ye, H. Q. A Free-Standing and Ultralong-Life Lithium-Selenium Battery Cathode Enabled by 3D Mesoporous Carbon/Graphene Hierarchical Architecture. *Adv. Funct. Mater.* **2015**, *25*, 455−463.
(56) Lukács, R.; Veres, M.; Shimakawa, K.; Kugler, S. On Photoinduced Volume Change in Amorphous Selenium: Quantum Chemical Calculation and Raman Spectroscopy. *J. Appl. Phys.* **2010**, *107*, 073517.
(57) Shen, W.; Wang, C.; Xu, Q. J.; Liu, H. M.; Wang, Y. G. Nitrogen-Doping-Induced Defects of a Carbon Coating Layer Facilitate Na-Storage in Electrode Materials. *Adv. Energy Mater.* **2015**, *5*, 1400982.
(58) Zhou, G. M.; Zhao, Y. B.; Manthiram, A. Dual-Confi ned Flexible Sulfur Cathodes Encapsulated in Nitrogen-Doped Double-Shelled Hollow Carbon Spheres and Wrapped with Graphene for Li−S Batteries. *Adv. Energy Mater.* **2015**, *5*, 1402263.
(59) Cui, Y.; Abouimrane, A.; Lu, J.; Bolin, T.; Ren, Y.; Weng, W.; Sun, C.; Maroni, V.; Heald, S.; Amine, K. (De) Lithiation Mechanism of Li/SeS_x (x= 0−7) Batteries Determined by in Situ Synchrotron X-ray Diffraction and X-ray Absorption Spectroscopy. *J. Am. Chem. Soc.* **2013**, *135*, 8047−8056.
(60) Babu, D.; Ramesha, K. Constraining polyselenide formation in ether based electrolytes through confinement of Se in microporous carbon matrix for Li-Se batteries. *Electrochim. Acta* **2016**, *219*, 295−304.
(61) He, X. M.; Ren, J. G.; Wang, L.; Pu, W. H.; Jiang, C. Y.; Wan, C. R. Expansion and Shrinkage of the Sulfur Composite Electrode in Rechargeable Lithium Batteries. *J. Power Sources* **2009**, *190*, 154−156.
(62) Shi, Y.; Wang, J. Z.; Chou, S. L.; Wexler, D.; Li, H. J.; Ozawa, K.; Liu, H. K.; Wu, Y. P. Hollow Structured Li_3VO_4 Wrapped with Graphene Nanosheets in Situ Prepared by a One-pot Template-free Method as an Anode for Lithium-ion Batteries. *Nano Lett.* **2013**, *13*, 4715−4720.
(63) Luo, C.; Zhu, Y. J.; Wen, Y.; Wang, J. J.; Wang, C. S. Carbonized Polyacrylonitrile-Stabilized SeS_x Cathodes for Long Cycle Life and High Power Density Lithium Ion Batteries. *Adv. Funct. Mater.* **2014**, *24*, 4082−4089.
(64) Wu, Y. P.; Jiang, C. Y.; Wan, C. R.; Fang, S. B.; Jiang, Y. Y. Nitrogen-containing Polymeric Carbon as Anode Material for Lithium Ion Secondary Battery. *J. Appl. Polym. Sci.* **2000**, *77*, 1735−1741.

DOI: 10.1021/acsami.7b04321
ACS Appl. Mater. Interfaces 2017, 9, 25232−25238